**Electronic Supplementary Information**

# A Multifunctional Phosphorylcholine-based Polymer Reduces Energy Loss for Efficient Perovskite Solar Cells

Lei Zhang,[a] Jiaxin Gao,[b] Zuhao You,[a] Qi Li,[a] Ming Liu,[a] Zaifei Ma[b] and Yao Liu*[a]

[a] State Key Laboratory of Chemical Resource Engineering, Beijing Advanced Innovation Center for Soft Matter Science and Engineering, Beijing University of Chemical Technology, Beijing 100029, China

[b] State Key Laboratory for Modification of Chemical Fibers and Polymer Materials, Center for Advanced Low-dimension Materials, College of Materials Science and Engineering, Donghua University, Shanghai, 201620, China

*Corresponding author.

*E-mail address:* liuyao@mail.buct.edu.cn

## Material synthesis

**Synthesis of PMPC**:

The RAFT agent 4-cyano-4- (ethylthiocarbonothioylthio) pentanoic acid (ECT) was synthesized according to the literature[1] Polymerization of MPC was carried out under[monomer]:[CTA]:[initiator]=500:10:1. MPC (0.50 g, 1.69 mmol), ECT (9.52 mg, 0.036 mmol), ACVA (1.01 mg, 0.0036 mmol) was dissolved in 0.5 M sodium chloride solution in water and titrated by 0.1 M sodium hydroxide solution in water. The solution was added to Schlenk tubes, then degassed by freeze-evacuate-thaw cycles three times. The tubes were heated under 70 °C for 24 h and the reaction was stopped by exposure to the air and cooled by water. The resulting solution was dialysis in water and lyophilization, giving the polymer as white solid. 1H NMR (400 MHz, D2O). δ (ppm) 4.25 (m, 2H), 4.18 (m, 2H), 4.04 (m, 2H), 3.64 (s, 6H), 3.19 (m, 2H), 2.03-1.80 (m, 2H), 1.35-0.75 (m, 3H). GPC: Mn: 17.2 kDa, Mw: 21.2 kDa, PDI:1.23

**Synthesis of PDI-NOH**:

3,4,9,10-perylenetetracarboxylic dianhydride (0.39 g, 1 mmol) was dispersed in *N*, *N*-dimethylformamide (15 mL) into a round bottom flask. The flask was evacuated and refilled with nitrogen several times. *N*-(3-Aminopropyl) diethanolamine (0.41 g, 2.5 mmol) was dissolved in N, N-dimethylformamide (DMF)and added slowly via syringe. The mixture was stirred at 90°C for 15 h and then poured into methanol. The precipitate was filtered off and washed with methanol and dichloromethane. After dried under vacuum, PDI-NOH was obtained as red solid (0.61g, 90 %); $^{1}$H NMR (400 MHz, DMSO-$d_6$) with a small amount of TFA-*d*, *δ*): 8.10 (d, *J* = 7.7 Hz, 4H), 8.02 (d, *J* = 7.7 Hz, 4H), 4.11 (s, 4H), 3.79 (t, *J* = 4.8 Hz, 8H), 3.29-3.40 (m, 12H), 2.17 (m, 4H); $^{13}$C NMR (100 MHz, DMSO-$d_6$ with a small amount of TFA-*d*, δ): 162.93, 133.33, 130.49, 127.82, 124.61, 123.98, 122.09, 55.62, 54.83, 51.58, 37.63, 22.47.

## Device Characterization and Measurement

Simulated AM 1.5G irradiation (100 mW cm$^{-2}$) was produced by a xenon-lamp-based Enli Solar Simulator for current-voltage (*J-V*) measurements. A Keithley 2400 Source Meter was used for driving the *J-V* measurement. The devices were measured immediately after fabrication without any preconditioning. A voltage scan was measured from -0.2 V to 1.2 V with a scanning rate

of 0.02 V $s^{-1}$. The EQE spectra were obtained using a QE-R system (Enli Tech, Taiwan) ranging from 300 nm to 900 nm under air condition. The device active area is 0.04 $cm^2$. All of the PSCs had no encapsulation. sEQE spectra were recorded by a highly sensitive home-built setup, which included a halogen lamp (LSH-75, Newport), an optical chopper, a monochromator (CS260-RG-3-MC-A, Newport), a phase-locked amplifier (SR830, Stanford Instrument) and a current amplifier (SR570, Stanford Instrument). The overtone signals from the monochromator were blocked by using a set of long pass filters (600 nm, 900 nm, 1100 nm). The size of the light beam from the monochromator was reduced to approximately 0.5 $mm^2$ by an optical aperture. EL spectra were measured using a source meter (Keithley 2400) to inject electric current into the solar cell device. A fluorescence spectrometer (KYMERA-3281-B2, Andor) with two sets of diffraction gratings, coupled to a Si EMCCD camera (DU970P-BVF, Andor, wavelength range of 400-1100 nm), and an InGaAs camera (DU491A-1.7, Andor, wavelength range of 900-1700 nm) was used to collect the photons emitted from the PSC devices. $EQE_{EL}$ measurements were carried out using a home-built setup: Electric current was injected into the solar cells by using a digital source meter (Keithley 2400), and the emitted photons were collected by a Si diode. The current generated by the Si diode was recorded by a picoammeters (Keithley 6482). Capacitance-voltage (C-V) curve of the complete PSCs were carried out for Mott-Schottky analysis by using CHI 660D electrochemical workstation with a frequency range from 2 MHz to10 Hz in the dark condition. Steady-state photoluminescence (PL) and time-resolved photoluminescence spectrum (TRPL) were recorded by FLS 980 spectrofluorometer (Edinburgh) with an excitation light of 405 nm and a pulsed excitation laser of 485 nm, respectively. The confocal laser scanning fluorescence microscopy was measured by ALR-SI03040100 (Nikon). Thin film X-ray diffraction (XRD) characterization of devices were measured using an D2 PHASER (Bruker) with Cu Kα (l = 0.154 nm) radiation in an angle range of 10-60°. X-ray photoelectron spectroscopy (XPS) was measured by Monochromatic Al Kα X-ray source ($hv$ = 1486.6 eV) of Thermo Scientific EACALAB $Xi^+$. Fourier transform

infrared (FTIR) spectra were obtained on a NICOLET 6700 spectrometer using KBr tablet technique. UV-*vis* absorption spectra were measured with a UV-*vis* spectrometer (UV-2600, SHIMADZU). Kelvin probe measurements were conducted by KP Technology Model SKP 5050. The top and section scanning electron microscope (SEM) were obtained by Zeiss Gemini SEM 360 working at a 10 kV. Atomic force microscopy (AFM) measurements were carried out in taping mode on Agilent AFM 5500.

***t*DOS measurement**

Moreover, the trap density of states (*t*DOS) was calculated using the equation:[2, 3]

$$N_T(E_\omega) = -\frac{V_{bi}\, dC\ \ \omega}{qWd\omega k_B T}$$

Where $V_{bi}$ is the built-in potential, C is the capacitance, $\omega$ is the angular frequency, q is the elementary charge, W is the depletion width (using the thickness of the active layer),[4] $V_{bi}$ is the built-in potential (extracted from the Mott-Schottky analysis), $k_B$ is the Boltzmann's constant and T is the temperature. The applied angular frequency ω is defined using the equation:[5]

$$E_\omega = k_B T \ln\left(\frac{\omega_0}{\omega}\right)$$

where $k_B$ is the Boltzmann's constant, $\omega_0$ is the characteristic transition angular frequency.

**TRPL measurement**

The PL decay curve is well fitted into a bi-exponential function:[6,7]

$$I_{(t)} = A_1 \cdot \exp\left(-\frac{t}{\tau_1}\right) + A_2 \cdot \exp\left(-\frac{t}{\tau_2}\right) + C$$

Where $A_1$, $A_2$ and C are constant, t is PL decay time, a fast decay ($\tau_1$) and a slow decay ($\tau_2$) are fitted lifetimes.

The average PL decay time $\tau_{average}$ is calculated by following equation:

$$\tau_{average} = \frac{A_1\tau_1^2 + A_2\tau_2^2}{A_1\tau_1 + A_2\tau_2}$$

**SCLC measurement**

SCLC measurement was applied to determine the hole trap density using the hole-only device with a configuration of ITO/PTAA@PMPC/perovskite (or perovskite: PMPC)/$MoO_3$/Au. $N_d$ in the perovskites can be calculated according to the equation:[8]

$$N_d = \frac{2\varepsilon\varepsilon_0 V_{TFL}}{eL^2}$$

Where $\varepsilon$ = 32,[9] $\varepsilon_0$ =8.85×10$^{-14}$ F cm$^{-1}$, and $e$ =1.6 ×10$^{-19}$ C are relative dielectric constant, vacuum permittivity, and elementary charge, respectively; L is the perovskite film thickness.

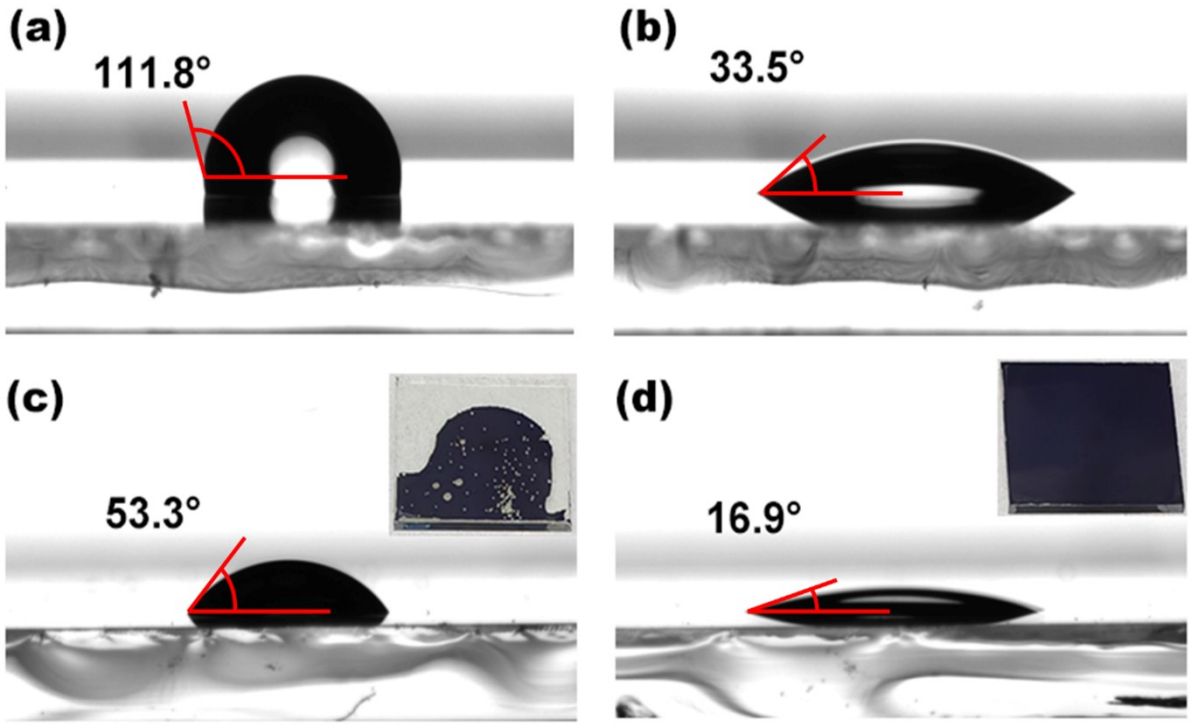


**Figure S1.** Contact angels of water on (a) PTAA and (b) PMPC@PTAA, contact angels of mix solvent (DMF/DMSO) on (c) PTAA and (d) PMPC@PTAA. The corresponding optical photos of perovskite films fabricated on different substrates are shown in inset.

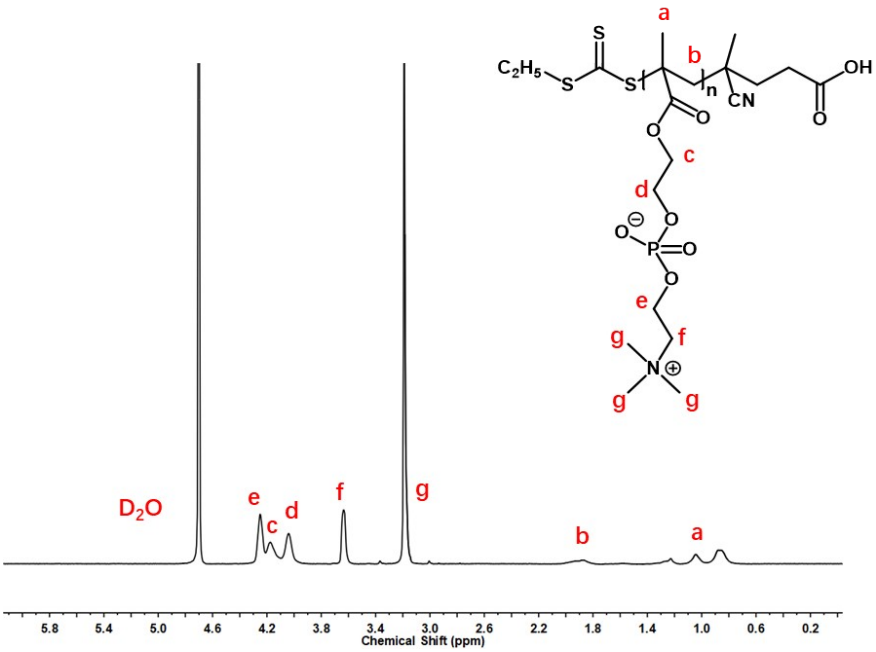


**Figure S2.** [1] H NMR spectrum of PMPC.

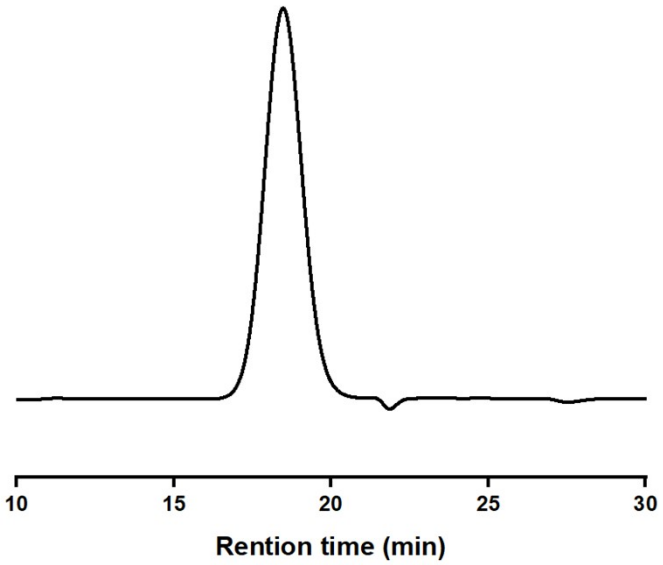


**Figure S3.** GPC spectrum of PMPC.

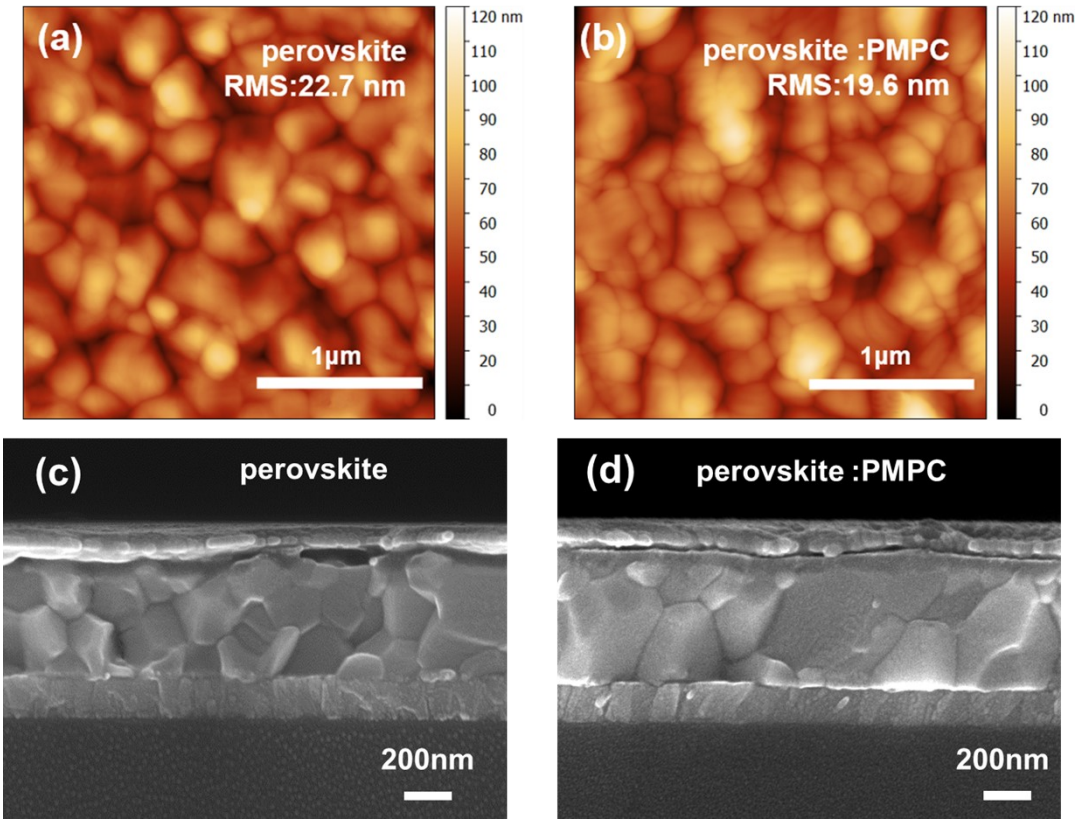


**Figure S4.** The atomic force microscope (AFM) images of (a) pristine perovskite and (b) perovskite: PMPC-based films, and cross-sectional SEM image of (c) pristine perovskite and (d) perovskite: PMPC-based films.

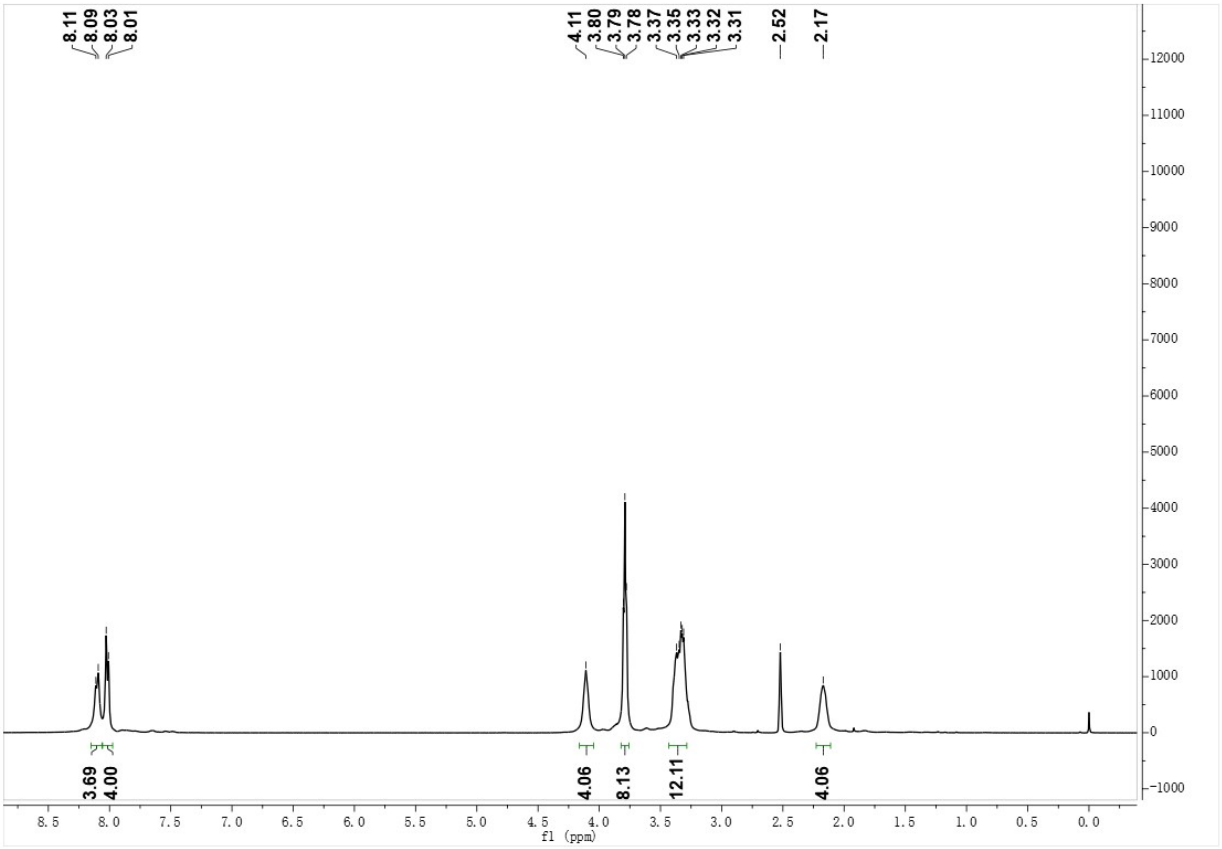


**Figure S5.** [1] H NMR spectrum of PDI-NOH.

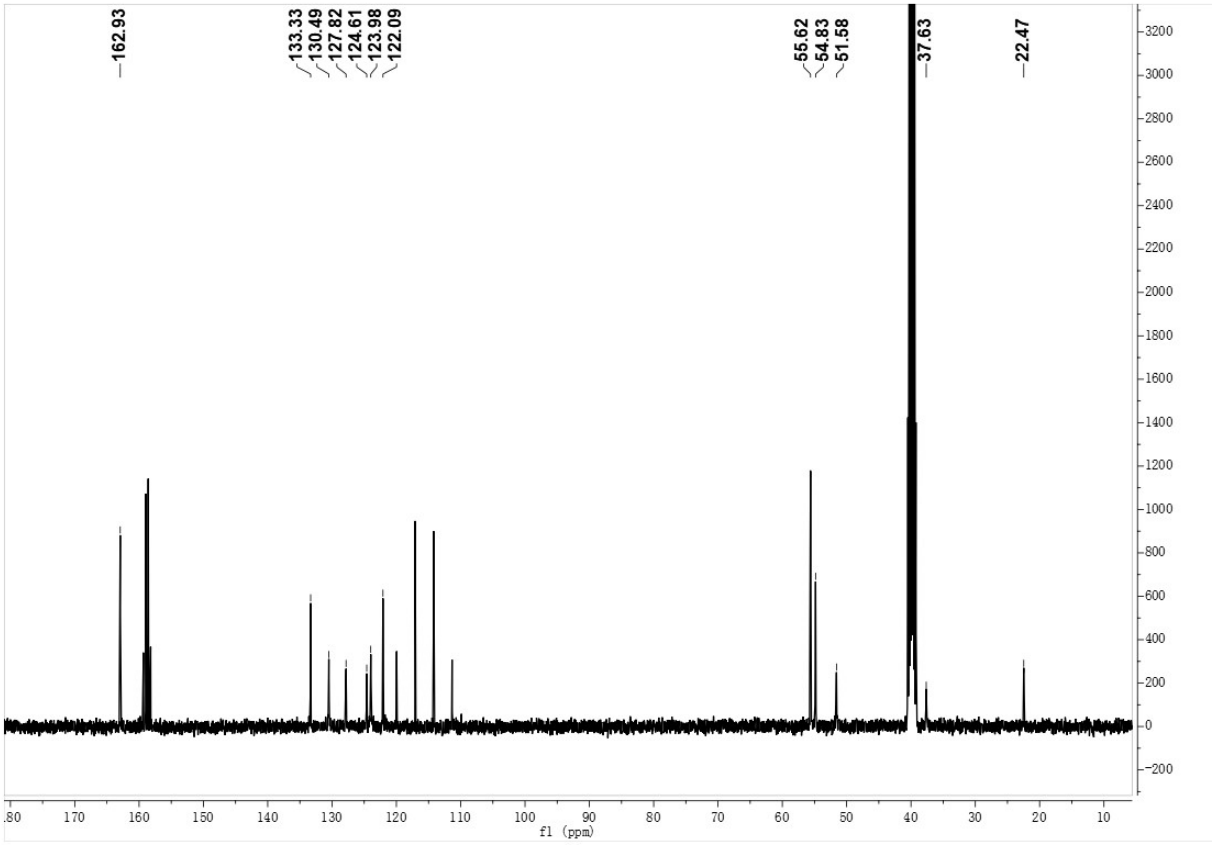


**Figure S6.** $^{13}$C NMR spectrum of PDI-NOH.

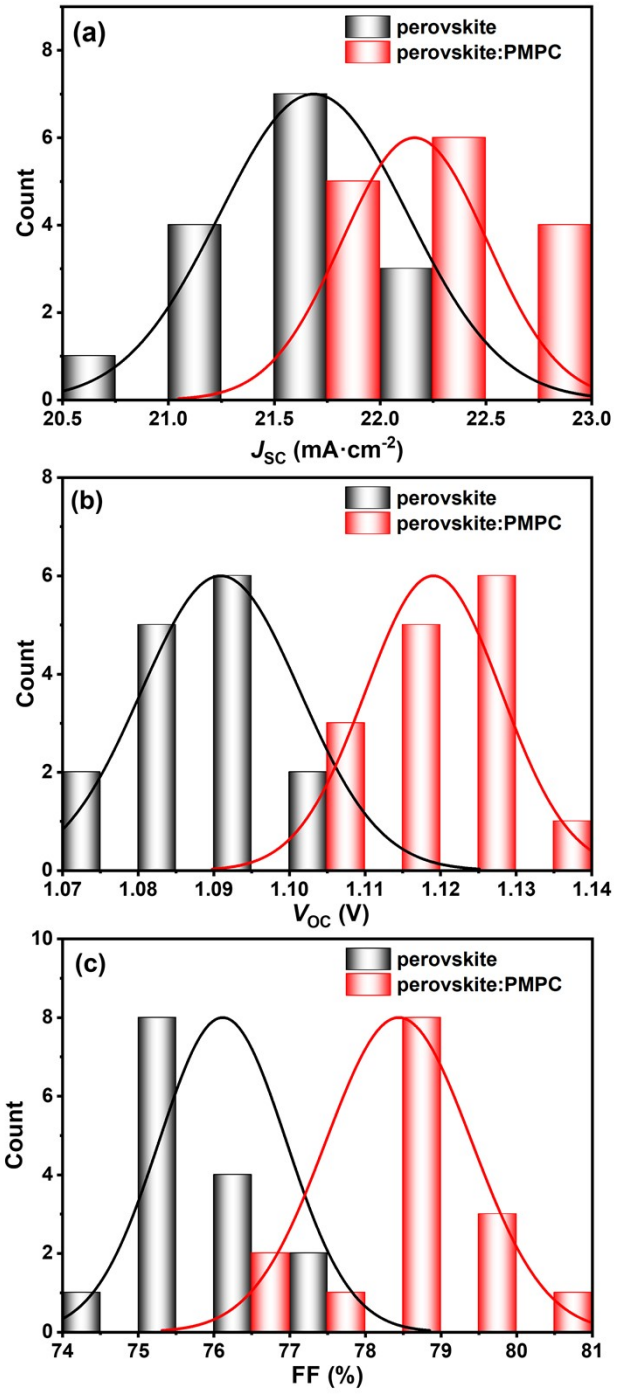


**Figure S7.** Photovoltaic parameter statistics of (a) $J_{SC}$, (b) $V_{OC}$, and (c) FF of pristine perovskite and perovskite: PMPC-based PSCs. 15 individual devices were used for statistical analysis.

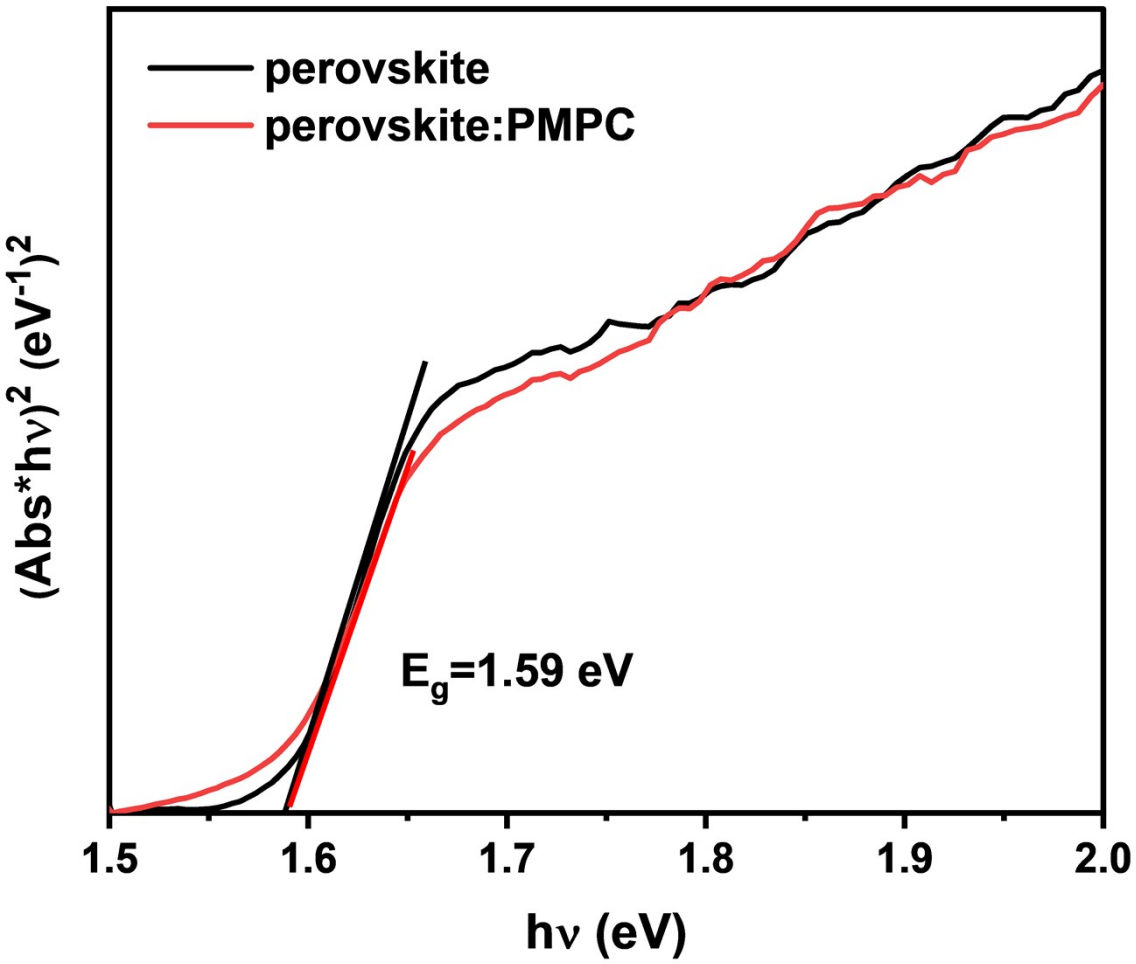


**Figure S8.** Tauc plots of the perovskite films with and without PMPC passivation from the UV-*vis* absorption spectra.

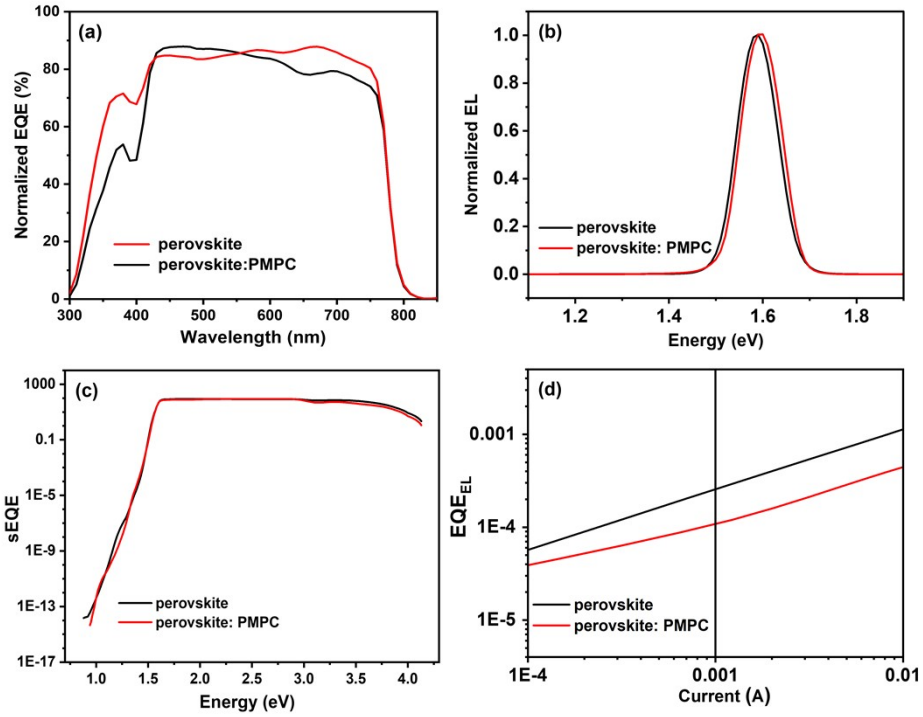


**Figure S9.** (a) EQE spectrum, (b) Normalized electroluminescence spectrum (EL), (c) $EQE_{PV}$ (sEQE), and (d) $EQE_{EL}$ for pristine perovskite and perovskite: PMPC-based PSCs, which used for calculating the values in Table 2.

**Table S1.** Summary of $V_{OC}$ loss of $MAPbI_3$ based PSCs containing different polymer or small molecule passivators.

| passivators | passivated device structure | PCE (%) | $V_{OC}$ loss (V) | Ref./Year |
|---|---|---|---|---|
| PMPC | ITO/PTAA@PMPC/$MAPbI_3$: PMPC/ $PC_{61}BM$/PDI-NOH/Ag | 20.2 | 0.48 | This work |
| PS | ITO/PTAA/$MAPbI_3$: PS/$PC_{61}BM$/BCP/Ag | 18.8 | 0.51 | 2020[10] |
| PCE-10 | ITO/PTAA/$MAPbI_3$: PCE-10/$PC_{61}BM$/BCP/Ag | 19.4 | 0.53 | 2020[10] |
| PASP | ITO/$P_3CT$-Na/PASP/$MAPbI_3$/$PC_{61}BM$/$C_{60}$/BCP/Ag | 20.0 | 0.52 | 2019[11] |
| PCBB-OEG | ITO/PTAA/$MAPbI_3$/PCBB-OEG/ $PC_{61}BM$ /Al | 20.2 | 0.52 | 2018[12] |
| PVC | ITO/PTAA/$MAPbI_3$: PVC/$PC_{61}BM$/Al | 18.7 | 0.52 | 2020[13] |
| PMMA | ITO/PTAA/PMMA/$MAPbI_3$/$PC_{61}BM$/ZrAcac /Ag | 19.5 | 0.49 | 2020[14] |
| PVPy | FTO/$TiO_2$/$MAPbI_3$/PVP/Spiro-OMeTAD/Au | 15.1 | 0.54 | 2017[15] |
| PEG | FTO/$TiO_2$/$MAPbI_3$: PEG/Spiro-OMeTAD/Au | ~16 | 0.57 | 2016[16] |
| TOPO | FTO/$TiO_2$/$ZrO_2$/Carbon (TOPO/$MAPbI_3$) | 12.8 | 0.63 | 2018[17] |
| F-PDI | ITO/$NiO_x$/$MAPbI_3$: F-PDI/ $PC_{61}BM$/BCP/Ag | 18.3 | 0.56 | 2019[18] |
| Rough FTO | FTO/$SnO_2$/$CH_3NH_3PbI_3$/Spiro-OMeTAD/Au | 20.4 | 0.37 | 2018[19] |
| OA | FTO/bl-$TiO_2$/mp-$TiO_2$/$MAPbI_3$: OA/PTAA/Au | 20.6 | 0.49 | 2018[20] |
| $GuaBF_4$ | ITO/$NiO_X$/$MAPbI_3$/$GuaBF_4$/$PC_{61}BM$/BCP/Ag | 20.54 | 0.49 | 2022[21] |
| Arginine | ITO/PTAA/$MAPbI_3$: Arg/ $PC_{61}BM$/BCP/Ag | 20.49 | 0.43 | 2021[22] |
| HTAB | ITO/PTAA/HTAB/$MAPbI_3$/$PC_{61}BM$/BCP/Ag | 21.01 | 0.48 | 2022[23] |
| MAOCN | ITO/TAPC/ $MAPbI_3$: MAOCN/PCBM/BCP/Ag | 21.28 | 0.47 | 2021[24] |

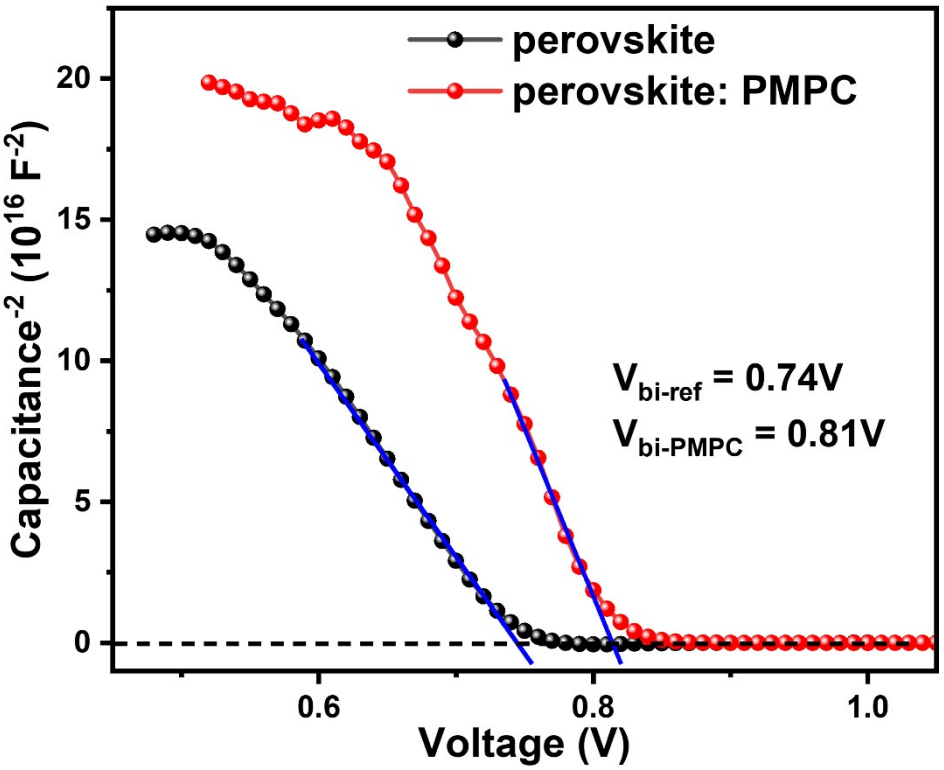


**Figure S10.** Mott-Schottky plots of devices with and without PMPC passivation measured at 1 kHz probe frequency.

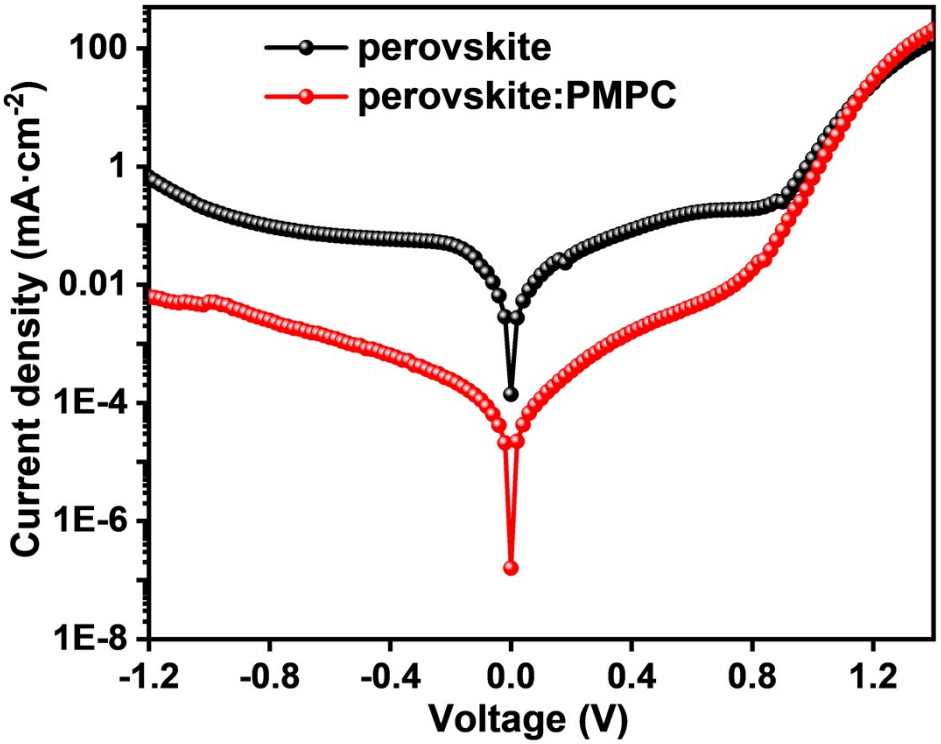


**Figure S11.** Dark *J*−*V* curves of the PSCs with and without PMPC passivation.

**Table S2.** Fitted parameters of the TRPL curve of perovskite and perovskite: PMPC films.

| Cells | $A_1$ | $\tau_1$ (ns) | $A_2$ | $\tau_2$ (ns) | $\tau_{average}$ (ns) |
|---|---|---|---|---|---|
| Perovskite | 0.78 | 3.29 | 0.34 | 68.55 | 61.98 |
| Perovskite: PMPC | 0.70 | 3.55 | 0.37 | 102.56 | 96.45 |

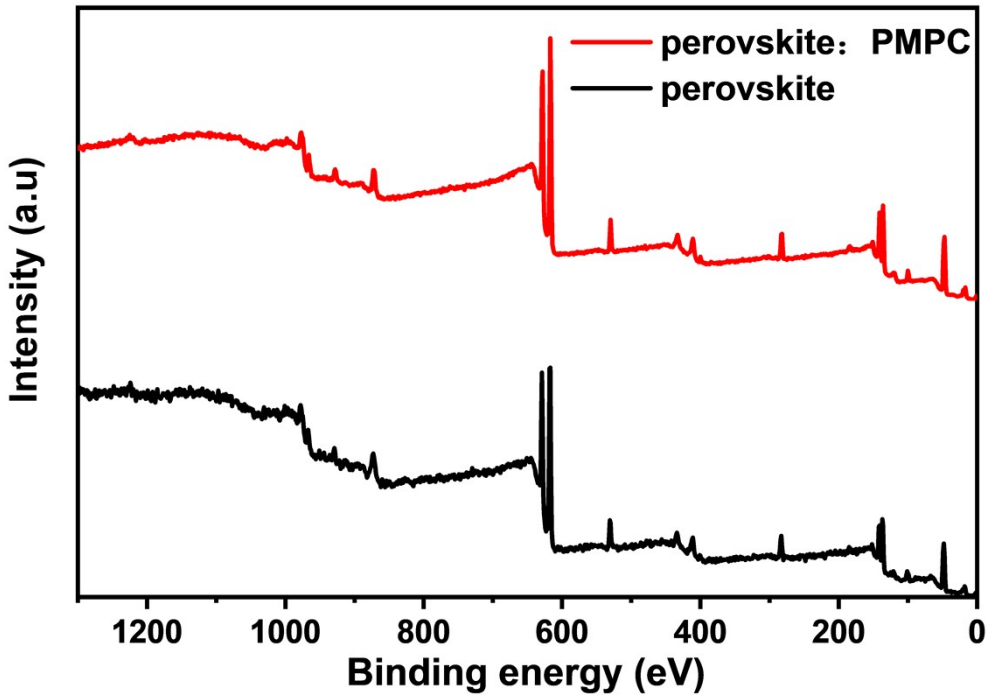


**Figure S12.** XPS survey spectra of pristine perovskite and perovskite: PMPC films.

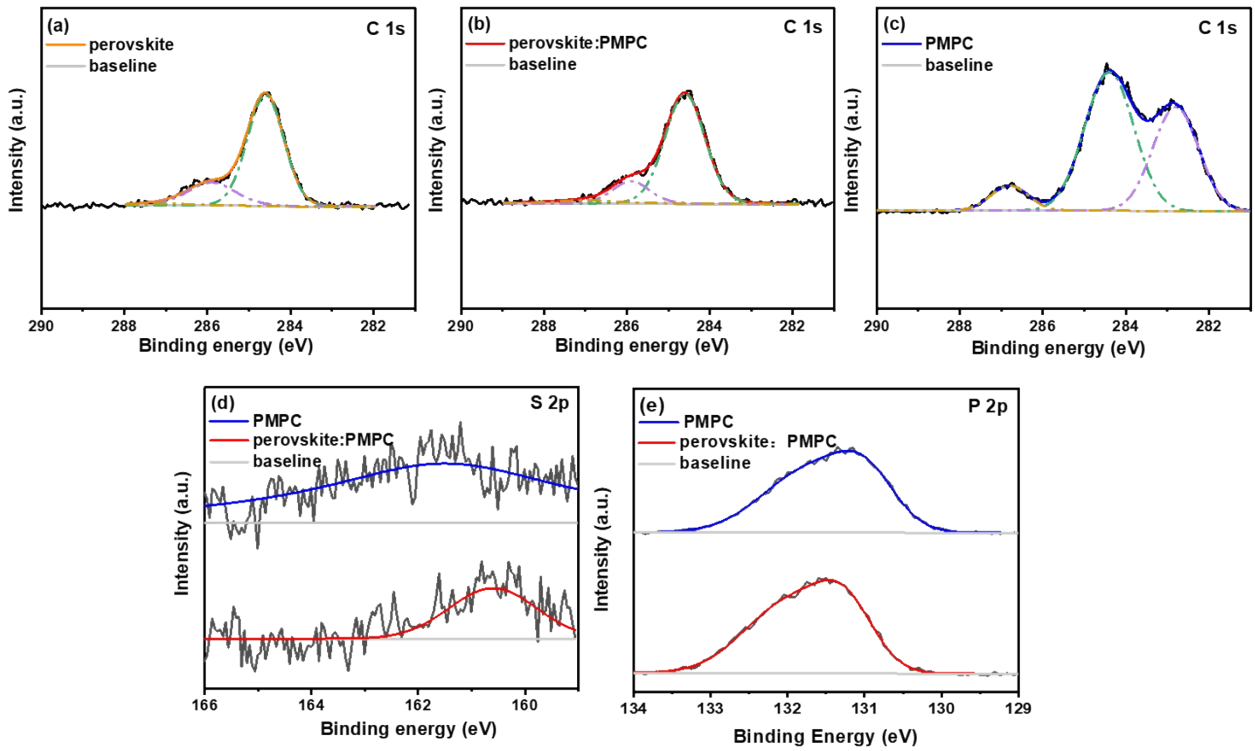


**Figure S13.** High-resolution XPS spectra of C1s for (a) perovskite, (b) perovskite: PMPC, (c) PMPC films; (d) S 2p and (e) P 2p for the PMPC and perovskite: PMPC films.

## Reference


1 T. Jin, M. Liu, K. Su, Y. Lu, G. Cheng, Y. Liu, N. W. Li and L. Yu, *ACS Appl. Mater. Interfaces*, 2021, **13**, 57489-57496.

2 M. Zi, X. Chen, S. Tan, C. Weng and B. Zhao, *Chem. Eng. J.*, 2022, **443**, 136455.

3 T. Walter, R. Herberholz, C. Müller and H. W. Schock, *J. Appl. Phys.*, 1996, **80**, 4411-4420.

4 Z. Li, Q. Shi, X. Ma, Y. Li, K. Wen, L. Qin, H. Chen, W. Huang, F. Zhang, Y. Lin, T. J. Marks and H. Huang, *Nat. Commun.*, 2022, **13**, 144-152.

5 J. A. Carr and S. Chaudhary, *J. Appl. Phys.*, 2013, **114**, 064509.

6 Q. Zhou, J. Qiu, Y. Wang, M. Yu, J. Liu and X. Zhang, *ACS Energy Lett.*, 2021, **6**, 1596-1606.

7 M. Jeong, I. W. Choi, E. M. Go, Y. Cho, M. Kim, B. Lee, S. Jeong, Y. Jo, H. W. Choi, J. Lee, J.-H. Bae, S. K. Kwak, D. S. Kim and C. Yang, *Science*, 2020, **369**, 1615-1620.

8 J. Chen, L. Zuo, Y. Zhang, X. Lian, W. Fu, J. Yan, J. Li, G. Wu, C.-Z. Li and H. Chen, *Adv. Energy Mater.*, 2018, **8**, 1800438.

9 Q. Dong, Y. Fang, Y. Shao, P. Mulligan, J. Qiu, L. Cao and J. Huang, *Science*, 2015, **347**, 967-970.

10 Y. Ma, Y. Cheng, X. Xu, M. Li, C. Zhang, S. H. Cheung, Z. Zeng, D. Shen, Y. M. Xie, K. L. Chiu, F. Lin, S. K. So, C. S. Lee and S. W. Tsang, *Adv. Funct. Mater.*, 2020, **31**, 2006802.

11 B. Wang, F. Wu, S. Bi, J. Zhou, J. Wang, X. Leng, D. Zhang, R. Meng, B. Xue, C. Zong, L. Zhu, Y. Zhang and H. Zhou, *J. Mater. Chem. A*, 2019, **7**, 23895-23903.

12 G. Xu, R. Xue, W. Chen, J. Zhang, M. Zhang, H. Chen, C. Cui, H. Li, Y. Li and Y. Li, *Adv. Energy Mater.*, 2018, **8**, 1703054.

13 L. A. Frolova, A. I. Davlethanov, N. N. Dremova, I. Zhidkov, A. F. Akbulatov, E. Z.

Kurmaev, S. M. Aldoshin, K. J. Stevenson and P. A. Troshin, *J Phys Chem Lett*, 2020, **11**, 6772-6778.

14 J. Wang, J. Xu, Z. Li, X. Lin, C. Yu, H. Wu and H.-l. Wang, *ACS Appl. Energy Mater.*, 2020, **3**, 6344-6351.

15 B. Chaudhary, A. Kulkarni, A. K. Jena, M. Ikegami, Y. Udagawa, H. Kunugita, K. Ema and T. Miyasaka, *ChemSusChem*, 2017, **10**, 2473-2479.

16 Y. Zhao, J. Wei, H. Li, Y. Yan, W. Zhou, D. Yu and Q. Zhao, *Nat. Commun.*, 2016, **7**, 10228.

17 G. Huang, C. Wang, H. Zhang, S. Xu, Q. Xu and Y. Cui, *J. Mater. Chem. A*, 2018, **6**, 2449-2455.

18 J. Yang, C. Liu, C. Cai, X. Hu, Z. Huang, X. Duan, X. Meng, Z. Yuan, L. Tan and Y. Chen, *Adv. Energy Mater.*, 2019, **9**, 1900198.

19 Y. Wang, Y. Liang, Y. Zhang, W. Yang, L. Sun and D. Xu, *Adv. Funct. Mater.*, 2018, **28**, 1801237.

20 M. Jung, T. J. Shin, J. Seo, G. Kim and S. I. Seok, *Energy Environ. Sci.*, 2018, **11**, 2188-2197.

21 B. Huang, X. Xia, X. Wang and F. Li, *Sol. Energy Mater Sol. Cells*, 2022, **240**, 111682.

22 J. Hu, X. Xu, Y. Chen, S. Wu, Z. Wang, Y. Wang, X. Jiang, B. Cai, T. Shi, C. J. Brabec, Y. Mai and F. Guo, *J. Mater. Chem. A*, 2021, **9**, 5857-5865.

23 Q. Sun, B. Zong, X. Meng, B. Shen, X. Li, B. Kang and S. R. P. Silva, *ACS Appl. Mater*, 2022, **14**, 6702-6713.

24 J. Tao, Z. Wang, H. Wang, J. Shen, X. Liu, J. Xue, H. Guo, G. Fu, W. Kong and S. Yang, *ACS Appl. Mater*, 2021, **13**, 44451-44459.